Water Resources Research

RESEARCH ARTICLE
10.1029/2020WR028126

Extreme Value Snow Water Equivalent and Snowmelt for Infrastructure Design Over the Contiguous United States

Eunsang Cho[1,2,3,4] **and Jennifer M. Jacobs**[1,2]

[1]Department of Civil and Environmental Engineering, University of New Hampshire, Durham, NH, USA, [2]Earth Systems Research Center, Institute for the Study of Earth, Oceans, and Space, University of New Hampshire, Durham, NH, USA, [3]Now at Hydrological Sciences Laboratory, NASA Goddard Space Flight Center, Greenbelt, MD, USA, [4]Now at Earth System Science Interdisciplinary Center, University of Maryland, College Park, MD, USA

Key Points:
- The 25- and 100-year design extreme SWE and snowmelt maps were developed by GEV probability distribution using the UA and SNODAS SWE
- The 7-day snowmelt exceeds the NOAA Atlas 14 standard design precipitation in 23% of the CONUS
- On average, the 25- and 100-year 7-day snowmelt with precipitation are 42 and 68 mm higher than those without precipitation, respectively

Supporting Information:
- Supporting Information S1

Correspondence to:
E. Cho,
ec1072@wildcats.unh.edu

Citation:
Cho, E., & Jacobs, J. M. (2020). Extreme value snow water equivalent and snowmelt for infrastructure design over the contiguous United States. *Water Resources Research*, *56*, e2020WR028126. https://doi.org/10.1029/2020WR028126

Received 9 JUN 2020
Accepted 6 SEP 2020
Accepted article online 12 SEP 2020

Abstract Snowmelt-driven floods result in large societal and economic impacts on local communities including infrastructure failures in the United States. However, the current U.S. government standard design precipitation maps are based on liquid precipitation data (e.g., National Oceanic and Atmospheric Administration's Precipitation-Frequency Atlas 14; NOAA Atlas 14) with very limited guidance on snowmelt-driven floods. In this study, we developed 25- and 100-year return level design maps of snow water equivalent (SWE) and 1- and 7-day snowmelt including precipitation events (e.g., rain-on-snow) using long-term observation-based gridded SWE developed by University of Arizona (UA) incorporating the national snow model product (SNOw Data Assimilation System; SNODAS) over the contiguous United States (CONUS). For the 44 U.S. states where the NOAA Atlas 14 maps are available, the design snowmelt values from this study exceed the standard design values in 23% of the total extent. The snowmelt values exceed the NOAA Atlas 14 design precipitation by up to 171 and 254 mm in the northeastern United States; 127 and 225 mm in the north central United States; and 191 and 425 mm in the western mountain United States for the 25- and 100-year return levels, respectively. A comparison of 7-day design snowmelt between with and without precipitation shows that including precipitation results in an average increase of 42 and 68 mm for 25- and 100-year return levels, respectively, over snowmelt that do not include precipitation. The design snowmelt maps from this study complement the NOAA Atlas 14 design precipitation and provide additional guidance on infrastructure design for snowmelt-driven floods in the CONUS.

Plain Language Summary Snow meltwater is a dominant driver of severe spring flooding in the north central and northeastern United States. Recent snowmelt floods, including rain-on-snow events, have resulted in large societal and economic impacts on local communities including infrastructure failures. The current U.S. government standard design precipitation maps are based on liquid precipitation data (e.g., NOAA Atlas 14 Volumes) with very limited guidance on snowmelt-driven floods. We developed 25- and 100-year return level design snow water equivalent (SWE) and snowmelt maps using the long-term observation-based gridded SWE incorporating the national snow model product over the contiguous United States. The design snowmelt values from this study exceed the Atlas 14 standard design values in 23% of the 44 U.S. states. In snow-dominant regions, the magnitudes of design snowmelt are much higher than the Atlas 14 design with precipitation increasing up to 191 and 425 mm for 25- and 100-year return levels, respectively. Results provide guidance in identifying areas and infrastructure vulnerable to snowmelt-driven floods.

1. Introduction

Snow and snowmelt driven extreme events can have large societal and economic consequences. Extreme snow can damage infrastructure and buildings (American National Standards Institute, 1972; American Society of Civil Engineers, 2017; Sack, 2015). Heavy snow loads on roofs can cause structural failures (Bean et al., 2019; Geis et al., 2012). From 1989 to 2009, 1,029 snow-induced building collapse incidents in the U.S. caused 19 fatalities and 146 injuries with each incident costing up to $200 million (Geis et al., 2012). In many parts of the U.S., snow meltwater is a dominant driver of severe spring flooding (Berghuijs

et al., 2016; Li et al., 2019). For example, Oroville dam's crisis in February 2017 in California was exacerbated by rapid snowmelt with a rain-on-snow (ROS) event (Henn et al., 2020; Musselman et al., 2018). Snowmelt floods routinely impact the north central and northeastern U.S. (Stadnyk et al., 2016; Tuttle et al., 2017; Wazney & Clark, 2015). The Red River of the North Basin's (RRB) 1997 snowmelt flood caused more than $5 billion of damage in Fargo and Grand Forks, North Dakota and other communities (Todhunter, 2001).

Civil engineers and water resources managers rely on historical precipitation data when making hydrologic estimates of design floods to size infrastructures (e.g., water management facilities, bridges, and other hydraulic control structures). The ability of infrastructure to withstand environmental stressors depends on the quality of input data. The National Oceanic and Atmospheric Administration's National Weather Service Precipitation-Frequency Atlas 14 (NOAA Atlas 14) series are the U.S. government standard to use in designing infrastructure with adequate capacity for flood events.

A large portion of peak flow events in snow-dominated regions of the United States is caused by snowmelt and ROS events (Berghuijs et al., 2016; Villarini, 2016). Berghuijs et al. (2016) explored the dominant flood-generating processes across the continental United States and found that snowmelt and ROS events were robust predictors of the flooding response compared to rainfall event only over the western, north central, and northeastern United States. Villarini (2016) regionalized flood-generating mechanisms across the continental United States based on the seasonality of flooding using 7,506 USGS stream gauge stations. They found that snowmelt is a major mechanism of flood generating in the Northern Great Plains and north-eastern United States. However, NOAA Atlas 14 guidance does not typically consider snow accumulation and melt events (Berghuijs et al., 2016; Bonnin et al., 2006). In a recent NOAA Atlas 14 document (Volume 10 Version 3.0), the authors attempted to subtract snowfall from the precipitation in order to calculate frequency estimates based on rainfall (i.e., liquid-only precipitation) only. From their limited analysis of three sites in the northeastern United States, Perica et al. (2015, revised 2019) concluded that differences between design estimates using rainfall only versus all precipitation estimates were inconsequential and thus no liquid-only precipitation frequency analysis was conducted.

In the western United States, recent studies showed that the magnitude of snowmelt frequently exceeded the standard NOAA guidance design values (Fassnacht & Records, 2015; Harpold & Kohler, 2017; Yan, Sun, Wigmosta, Leung, et al., 2019; Yan, Sun, Wigmosta, & Skaggs, 2019). Harpold and Kohler (2017) found that only 21% of mountain locations had a 100-year return level, 24-hr intensity caused by rainfall during the snow-free period, indicating the remainder result from snowmelt and ROS events. The magnitude of snowmelt exceeded the standard NOAA precipitation design values at 78 of the 379 Snowpack Telemetry (SNOTEL) stations (21%). Across the southern Rocky Mountains, the 24-hr snowmelt intensity exceeded the 24-hr rainfall intensity by 53% and 38% for 10- and 100-year events, respectively (Fassnacht & Records, 2015). Yan et al. (2018) stated that snowmelt and ROS events exceeded precipitation at 127 and 142 out of the 376 Snowpack Telemetry (SNOTEL) stations for 10 and 100 years, 24-hr events, and proposed the next-generation intensity-duration-frequency (NG-IDF) curves incorporating snowmelt and ROS events to overcome the deficiency of precipitation-based IDF curves. Yan, Sun, Wigmosta, Leung, et al. (2019) and Yan, Sun, Wigmosta, & Skaggs (2019) evaluated the performance of the NG-IDF curves using a physical-based hydrological model. They showed a reduction of the averaged error for the 50-year flood with the use of NG-IDF curves (12%) as compared to the use of precipitation-based IDF curves (31%). They stated that ~70% of the SNOTEL stations have the potential for underdesigned flood estimates across the western United States (Yan, Sun, Wigmosta, & Skaggs, 2019).

To accurately estimate the magnitude of snowmelt events regions of the CONUS with a seasonal snowpack, a reliable, spatially distributed SWE record is required. Spatially distributed SWE products have been developed using assimilation techniques by ingesting in situ snow station networks and remotely sensed snow products over the CONUS (Barrett, 2003; Broxton, Dawson, & Zeng, 2016; Carroll et al., 2006; Takala et al., 2011). The SNOw Data Assimilation System (SNODAS) operated by the National Weather Service (NWS) National Operational Hydrologic Remote Sensing Center (NOHRSC) provides a near-real-time 30 arc-second grid (about 1 km^2) of spatially distributed SWE throughout the continental United States [CONUS] (Barrett, 2003). The SNODAS data provide the only real-time spatially distributed estimate of snowpack conditions across the CONUS and are used operationally by hydrologists and flood forecasters

in regional NOAA river forecast centers. Unfortunately, the SNODAS SWE data record, September 2003 to current (16 winters), is too short to be used to estimate extreme snowmelt events.

Recently, the University of Arizona (UA) released a long-term gridded (4 km) daily SWE data set (hereafter UA SWE) over the CONUS for the period October 1981 to May 2017 through the NASA National Snow and Ice Data Center (Broxton, Zeng, & Dawson, 2016). UA SWE was produced by assimilating the Parameter-elevation Regressions on Independent Slopes Model (PRISM) daily precipitation and temperature data developed by the PRISM Climate Group at Oregon State University (Daly et al., 2008), SWE and snow depth data from the SNOTEL network (Serreze et al., 1999), and SWE and snow depth data from the NWS Cooperative Observer Program (COOP) network. Broxton et al. (2016) found that UA SWE has similar spatial and temporal variability as SNODAS SWE, while the reanalysis and GLDAS products substantially underestimate SWE compared to the two SWE products. Dawson et al. (2018) showed that UA SWE had a strong agreement with Airborne Snow Observatory (ASO) SWE products over the Toulumne basin in California. Cho et al. (2019) demonstrated that the UA SWE had the best agreement with historical airborne gamma radiation SWE observations ($N = 20{,}738$ observations from 1982 to 2017) as compared to GlobSnow-2 and microwave satellite SWE, regardless of snow classification and land cover type.

The availability of the complementary and well-vetted SNODAS and UA SWE products provides a unique opportunity to inform the engineering design of structures and facilities that must withstand snow loads or snowmelt runoff. Here we seek to draw from the strengths of these two SWE products, UA SWE and SNODAS SWE, to develop design values for SWE and snowmelt over the CONUS that are needed to support a range of engineering design needs. This is achieved by, first, analyzing the systematic differences (i.e., bias) in extreme SWE and snowmelt between UA and SNODAS data sets; second, bias correcting and detrending UA SWE using the SNODAS data via empirical cumulative distribution function (ECDF) method (McGinnis et al., 2015) and traditional detrending techniques (Sen, 1968); and finally, conducting an extreme value frequency analysis in which historical annual maximum is used to fit the generalized extreme value (GEV) probability distribution (Bonnin et al., 2006; Cheng & AghaKouchak, 2014; Perica et al., 2013, 2015) and the fitted distribution is used to map annual maximum SWE and snowmelt for various return periods.

The subsequent sections are organized as follows. Section 2 explains the SNODAS and UA SWE data sets. Section 3 describes the methodologies including identification of the annual maximum 1- and 7-day snowmelt events, bias correcting and detrending, and application of the extreme value methods. Section 4 compares the annual maximum SWE and snowmelt from UA and SNODAS products, identifies annual maximum SWE and snowmelt trends, presents the 25- and 100-year design SWE and snowmelt maps, and compares these maps to the current NOAA Atlas 14 maps. Section 5 discusses results in light of previous work and presents potential limitations in the approach. Conclusion and future perspectives appear in section 6.

2. Data

2.1. SNODAS SWE and Precipitation

In this study, SNODAS products are used as the benchmark. SNODAS products are well vetted by previous research throughout the United States (Broxton, Zeng, & Dawson, 2016; Schroeder et al., 2019; Vuyovich et al., 2014) and have been used operationally by hydrologists and flood forecasters in the regional river forecast centers for the entire United States (Carroll et al., 2006). NOAA's SNODAS integrates model results with ground observations, airborne gamma SWE, and satellite snow cover estimates, to generate the best 1 km gridded estimate of the snow characteristics that minimize errors associated with any individual method (Carroll et al., 2006). The three main procedures in the SNODAS ingest and downscale numerical weather prediction (NWP) output, simulate the snowpack using a physically based energy and mass balance model, and assimilate independent satellite, airborne, and ground-based observations of snow cover area (SCA) and SWE to adjust model results. Forcing data comes from the Rapid Update Cycle 2 (RUC2) NWP output generated by the National Centers for Environmental Prediction (NCEP) and are downscaled using a digital elevation model. The snow model is energy and mass balance, multilayer model and consists of three snow layers and two soil layers (Barrett, 2003). For the assimilation procedure, snow observations include ground station-based SWE and airborne gamma radiation SWE as well as satellite-based SCA information.

SNODAS V1 data are freely available from the NASA National Snow and Ice Data Center from 1 October 2003 to the present (https://nsidc.org/data/g02158). In this study, the original, daily SNODAS SWE and solid and liquid precipitation data (1 km × 1 km spatial grid) were used from 1 October 2003 to 31 May 2017 (14 water years). The original SNODAS data were aggregated to 4-km grid by using the average function and then resampled to match the grid location of the upscaled SNODAS to that of UA data (4 km × 4 km spatial grid) using the nearest neighbor method. The errors introduced by the nearest neighbor method were minimal as compared to other resampling options (e.g., bilinear interpolation).

2.2. UA SWE

The observation-based 4 km UA SWE combines station-based SWE and snow depth observations with a background modeled SWE using an empirical temperature index snow model over the CONUS (Broxton et al., 2019; Broxton, Dawson, & Zeng, 2016). The station-based SWE and snow depth observations are from the Snowpack Telemetry (SNOTEL) network and the National Weather Service Cooperative Observer Program (COOP) network, respectively. The background modeled SWE was generated using the PRISM precipitation and temperature data as forcing data into an empirical temperature index snow model (Broxton, Dawson, & Zeng, 2016). The quality of the UA SWE data was evaluated with the current reanalysis and the Global Land Data Assimilation System (GLDAS)-based land surface model products (Broxton, Zeng, & Dawson, 2016). A summary of recent updates in the UA product with trend/driver analysis of the data was provided in Zeng et al. (2018). The UA SWE data (Version 1) was recently released and freely available at NASA National Snow and Ice Data Center from 1 October 1981 to 30 September 2017 (https://nsidc.org/data/nsidc-0719). In this study, daily 4 km gridded UA SWE values were used from October 1981 to May 2017 (36 water years). To calculate UA annual maximum snowmelt with precipitation (e.g., ROS events), the daily 4 km gridded PRISM precipitation values were used for the same period. The daily PRISM data were obtained using the "get_prism_dailys" function in the "prism" R package (https://github.com/ropensci/prism).

2.3. NOAA Atlas 14 Precipitation Frequency Estimates

The NOAA Atlas 14 includes design precipitation estimates for selected durations and frequencies as well as the lower and upper bounds of the 90% confidence interval for the United States. Atlas 14 also contains supporting information on methodologies and results of trend and seasonal analyses. The Atlas 14 precipitation frequency estimates are determined from long-term precipitation records from a regional network of rainfall gauges (Bonnin et al., 2006; Perica et al., 2013, 2015). In this study, the recent Atlas 14 precipitation frequency CONUS maps are compared to this study's design snowmelt maps, except for northwestern United States and Ohio River Basin. The NOAA Atlas 14 maps are not available over the northwestern U.S. region. While Atlas14 Volume 2 provides design precipitation values for the Ohio River Basin and surrounding states, the annual maximum series for that region are not available. The Atlas 14 precipitation spatial maps at a 1 km spatial grid are available from the Hydrometeorological Design Studies Center (HDSC) within the Office of Water Prediction (OWP) of the NOAA's National Weather Service (NWS) (https://hdsc.nws.noaa.gov/hdsc/pfds/pfds_gis.html). The 1 km Atlas 14 maps were aggregated/resampled to spatially match the UA SWE data (4 km × 4 km spatial grid) using the nearest neighbor method.

3. Methodology

3.1. Annual Maximum SWE and Snowmelt

All available gridded, daily time series of UA and SNODAS SWE with PRISM and SNODAS precipitation data were used to obtain the annual maximum SWE and snowmelt values for 36 and 14 water years, respectively. Annual maximum SWE values are the 1-day maximum value determined for each pixel using the 1 October to 30 May SWE daily time series. For snowmelt, 1- and 7-day design snowmelt including precipitation were calculated. The 1-day (24-hr) duration is a typical storm duration for hydrologic design manuals (Yan et al., 2018; Yan, Sun, Wigmosta, Leung, et al., 2019; Yan, Sun, Wigmosta, & Skaggs, 2019). Infrastructure with a large amount of available storage (e.g., dams) may not be impacted by a short-duration event, and a longer-duration event should be considered in design (Federal Emergency Management Agency, 2012). Ivancic and Shaw (2015) found 5 days or longer lag times between streamflow and snowmelt response across the U.S. snow-dominant watersheds. Davenport et al. (2020) used a streamflow response to precipitation events as 8-day window across the western United States. Therefore, the 7-day duration is used

on design snowmelt in this study. Complete 7-day snowmelt results are presented in the body of the paper, and additional 1-day snowmelt results are included in the supporting information.

For example, annual maximum 7-day snowmelt including precipitation ($Melt_{max,\,7d}$) for each pixel is defined as

$$Melt_{max,\,7} = \max[PREC_{i+1\ to\ i+7} - (SWE_i - SWE_{i+7})] \text{ when } SWE_i - SWE_{i+7} > 0 \quad (1)$$

where i is a date from 1 October to 31 May for each water year, and SWE_i and SWE_{i+7} is daily SWE (mm) at dates, i and $i + 7$, respectively. $PREC_{i+1\ to\ i+7}$ is accumulated precipitation (mm) between i and $i + 7$ dates. To consider snow-driven events only, the annual maximum snowmelt value is selected when $SWE_i - SWE_{i+7}$ (ΔSWE) at i date is positive only (e.g., snow ablation). This equation is based on the mass balance of snowpack, Melt (output) = Precipitation (input) – ΔSWE (storage change). In this study, "snowmelt" includes the actual amount of water available for runoff from melting snow and precipitation for the runoff process (Yan et al., 2018).

The study period is divided into two periods: the period where both UA and SNODAS data are available (14 years; WY2004–WY2017) and the period during which only UA SWE is available (22 years; WY1982–WY2003). The annual maximum snowmelt data for the 14 years with concurrent data were used to determine a statistical relationship between UA and SNODAS. All pixels having extremely low mean annual maximum SWE (<2.54 mm) for either UA and SNODAS products (e.g., south of Arizona and Texas and Louisiana) are excluded from this work because 0.54 mm or 0.1 inch of SWE is the minimum measurement uncertainty from stations (Musselman et al., 2017).

3.2. ECDF

The SNODAS SWE is widely considered to be the most reliable gridded SWE product over the CONUS (Barrett, 2003; Broxton, Zeng, & Dawson, 2016). The ECDF method was applied to bias correct the UA annual maximum SWE and snowmelt data using SNODAS annual maximum SWE and snowmelt. The ECDF is widely used in climate modeling to correct systematic model bias based on observation data (McGinnis et al., 2015). In this study, CDFs of the UA annual maximum SWE and snowmelt values, $CDF_{UA_{14}}$, for the period where both UA and SNODAS data are available (14 years; WY2004–WY2017) are used to determine probabilities associated with the UA annual maximum SWE or snowmelt values. The bias correction technique transforms these probabilities back into snowmelt values using the inverse CDF of the SNODAS distribution developed for the 14 years, $CDF^{-1}_{SNODAS_{14}}$, as follows:

$$ECDF^{-}Melt_{UA_i} = CDF^{-1}_{SNODAS_{14}}(CDF_{UA_{14}}(Melt_{UA_i})), \quad if\ Melt_{UA_i} \le \max(Melt_{UA_{14}}) \quad (2)$$

where $ECDF^{-}Melt_{UA_i}$ and $Melt_{UA_i}$ are given as the ECDF transformed annual maximum snowmelt event and the original annual maximum snowmelt at year i, respectively, and $\max(Melt_{UA_{14}})$ is the maximum snowmelt in the overlapping 14 years.

If a UA value at year i, $Melt_{UA_i}$, exceeded the maximum UA of the 14 years, $\max(Melt_{UA_{14}})$, a difference between the UA value and the maximum UA multiplied by a ratio of the standard deviation of the UA snowmelt, $\mathrm{std}(Melt_{UA_{14}})$, to that of SNODAS snowmelt, $\mathrm{std}(Melt_{SNODAS_{14}})$, was added in the maximum SNODAS values of the 14-year periods, $\max(Melt_{SNODAS_{14}})$, as follows:

$$ECDF^{-}Melt_{UA,\,i} = \max(Melt_{SNODAS_{14}}) + \left[Melt_{UA,\ \ i} - \max(Melt_{UA_{14}})\right]\frac{\mathrm{std}(Melt_{SNODAS_{14}})}{\mathrm{std}(Melt_{UA_{14}})}, \quad if\ Melt_{UA_i} > \max(Melt_{UA_{14}}) \quad (3)$$

3.3. Trend Identification and Detrend Method

Because stationarity is an underlying assumption of most frequency analyses that develop estimates of extreme values (Khaliq et al., 2006), a trend analysis was conducted for each pixel's time series and time series having significant trends were detrended. The nonparametric Mann-Kendall test was used to identify statistically significant trends (5% confidence level) in the historical annual maximum SWE and snowmelt values (Kendall, 1938; Mann, 1945). If a significant trend in an annual maximum time series was found

for a given pixel, each value in the time series was detrended using Sen's slope of the trend maintaining the time series' average (Fassnacht & Records, 2015; Sen, 1968; Yan et al., 2018) before fitting the extreme value distribution.

3.4. GEV Distribution

In this study, SWE and snowmelt magnitude-frequency estimates at individual grid cells are computed using the GEV-based frequency analysis approach based on L moment statistics (Hosking et al., 1985). The GEV distribution is fitted using the annual maximum series of SWE and 7-day snowmelt and then used to estimate the 25- and 100-year return period SWE and 7-day snowmelt design values. The GEV distribution incorporates three types of extreme value distributions, Gumbel, Fréchet, and Weibull distributions. The cumulative distribution function of the GEV can be written as

$$F(x) = \exp\left\{-\left[1 - \frac{\kappa(x-\xi)}{\alpha}\right]^{\frac{1}{\kappa}}\right\} \text{ for } \kappa \neq 0 \tag{4}$$

where the location parameter (ξ) represents the center of the GEV distribution, the scale parameter (α) specifies the deviation around ξ, and the shape parameter (κ) determines the tail behavior of the distribution. The Gumbel distribution is obtained when $\kappa = 0$. For $\kappa > 0$, the GEV corresponds to the Fréchet distribution. For $\kappa < 0$, the GEV leads to the Weibull distribution which has a thicker right-hand tail. The parameters of the GEV distribution are

$$\kappa = 7.8590c + 2.9554c^2,\ \mathrm{c} = \frac{2\lambda_2}{\lambda_3 + 3\lambda_2} - \frac{\ln(2)}{\ln(3)} \tag{5}$$

$$\alpha = \frac{\kappa\lambda_2}{\Gamma(1+\kappa)(1-2^{-\kappa})} \tag{6}$$

$$\xi = \lambda_1 + \frac{\alpha}{\kappa}[\Gamma(1+\kappa) - 1] \tag{7}$$

where λ_1,λ_2, and λ_3 are the first, second, and third L moments, respectively, and $\Gamma()$ is the gamma function (Hosking et al., 1985; Stedinger et al., 1993). L moments provide an alternative approach of describing the shape of probability distributions to conventional moments or maximum likelihood approach (Hosking, 1990). Because sample estimators of L moments are linear combinations of ranked data, the L moments are less susceptible to outliers than conventional moments (Vogel & Fennessey, 1993). They are also well suited for analyzing the data with significant skewness.

For pixels having some years with zero values, the zero values were considered to be NA values (so called "censored data") and a conditional probability model was employed. In this case, only the positive, nonzero values were included in the L moments calculations used to fit the GEV distribution $G(x)$. An additional parameter (P_o) was included to describe the probability that the SWE is zero. For pixels with the censored data, the nonexceedance probability of the GEV distribution was adjusted by a portion of the censored data (Stedinger et al., 1993) such that the unconditional cumulative distribution function $F(x)$ for any value of SWE greater than zero is given as

$$F(x) = P_0 + (1 - P_0) \cdot G(x) \tag{8}$$

For example, if there were zero values in 9 years out of 36 years, the nonexceedance probability, $G(x)$, was multiplied by a portion of the censored data ($P_0 = 9/36 = 0.25$, $1 - P_0 = 0.75$ in this case) and then added to P_0. If nonexceedance probabilities for 25- and 100-year return levels are 0.96 and 0.99, then the unconditional nonexceedance probabilities, $F(x)$, are 0.97 and 0.9925. If 50% or more of a pixel's data set was zero values, then the pixel was excluded from this study.

The goodness-of-fit of the GEV model was examined by the probability plot correlation coefficient (PPCC) test using R package. The PPCC test, developed by Filliben (1975) and Looney and Gulledge (1985), is defined as the product moment correlation coefficient between the ordered data and the order statistic medians. If the data are drawn from the hypothesized GEV distribution, the correlation coefficient will be near to

one and the plot is expected to be nearly linear (Chowdhury et al., 1991). In this study, the annual maximum SWE and 1- and 7-day snowmelt time series data excluding the censored data were tested for each pixel. When a pixel's time series was not rejected as being from the GEV distribution based on the PPCC test with 0.05 significant level, the pixel was used for developing GEV distribution and extreme values with 25- and 100-year return levels. If the GEV distribution was rejected, the extreme SWE and snowmelt values were excluded in this analysis.

4. Results

4.1. Comparison of Annual Maximum SWE and Snowmelt Between UA and SNODAS

Before developing the design extreme values, the UA-based annual maximum SWE and snowmelt were compared to that of SNODAS for the overlapping period of record (October 2003 to May 2017). Figure 1 shows maps of the mean annual maximum SWE and snowmelt produced from the UA and SNODAS SWE with precipitation data. To support this figure, Table 1 provides statistics of the mean annual maximum SWE and snowmelt by state (spatial mean, standard deviation, and 99% quantiles). The two UA annual maximum products show similar spatial patterns over the CONUS with the SNODAS products. The difference maps reveal that SNODAS annual maximum SWE is generally somewhat higher than the UA annual maximum SWE values in the north-central United States and nonmountain western United States. However, in the Great Lakes and northeastern regions, UA annual maximum SWE occasionally exceed SNODAS annual maximum SWE.

In the western United States, both annual maximum SWE data sets have high mean values and large standard deviations due to the spatially heterogeneous regions. Based on the SWE difference map (Figure 1e), differences are mixed especially in the mountainous areas. For example, state-mean values of UA are 189, 206, and 111 mm, and SNODAS, 202, 213, and 121 mm (standard deviations: 321, 211, and 176 mm for UA and 322, 220, and 179 mm for SNODAS) in Washington, Idaho, and Wyoming, respectively (Table 1). The 99% quantile values, characterizing deep SWE in those states' mountain areas, are 1,439, 886, and 797 mm from UA and 1,363, 943, and 753 mm from SNODAS. While the state-mean values of UA are slightly lower than the values of SNODAS, the 99% quantile UA values are higher than the SNODAS values in most western U.S. states (e.g., Washington, Wyoming, Montana, Colorado, and Utah).

In the northeastern regions, UA annual maximum SWE is much higher than that from SNODAS with UA's state-mean SWE values of 203, 167, and 166 mm as compared to SNODAS values of 177, 132, and 131 mm, for Maine, New Hampshire, and Vermont, respectively. Not surprisingly, the standard deviations in the northeast are much lower than the western regions with UA and SNODAS having similar variability (UA: 46, 61, and 53 mm and SNODAS: 57, 49, and 44 mm). The SNODAS 99% quantile values, 289, 268, and 235 mm, are similar to the state-mean values indicating that there is relatively little spatial variation in the eastern United States.

In the north-central United States, the annual maximum SWE from both products is relatively low compared to the other regions. The state-mean values of SNODAS range from 49 to 89 mm with the 99% quantile values from 84 to 228 mm, while UA state-mean values range from 37 to 99 mm and 99% quantile values range from 71 to 219 mm. The SNODAS annual maximum SWE is generally higher than UA product in these regions (e.g., Northern Great Plains).

The annual maximum 7-day snowmelt spatial patterns are similar to the annual maximum SWE patterns where the largest snowmelt events occur in the western mountainous regions, followed by northeastern, then Great Lakes region. SNODAS annual maximum snowmelt values are generally higher than UA values in the nonmountainous areas over the CONUS. UA snowmelt is much higher than SNODAS in the western mountainous areas where the differences between UA and SNODAS snowmelt values reach up to 300 mm.

At a state level, the northeastern states have the largest state-mean snowmelt (e.g., UA: 127, 120, and 113 mm; SNODAS: 137, 114, and 108 mm for Maine, New Hampshire, and Vermont, respectively). In the north central United States, the state-mean SNODAS snowmelt values, 72, 64, and 54 mm, are consistently larger than the UA snowmelt values, 61, 44, and 36 mm for Minnesota, North Dakota, and South Dakota, respectively. The 99% quantile values have similar differences between two products to the state-mean snowmelt values in the regions (7, 22, and 20 mm for the states, respectively). In the western United States, the

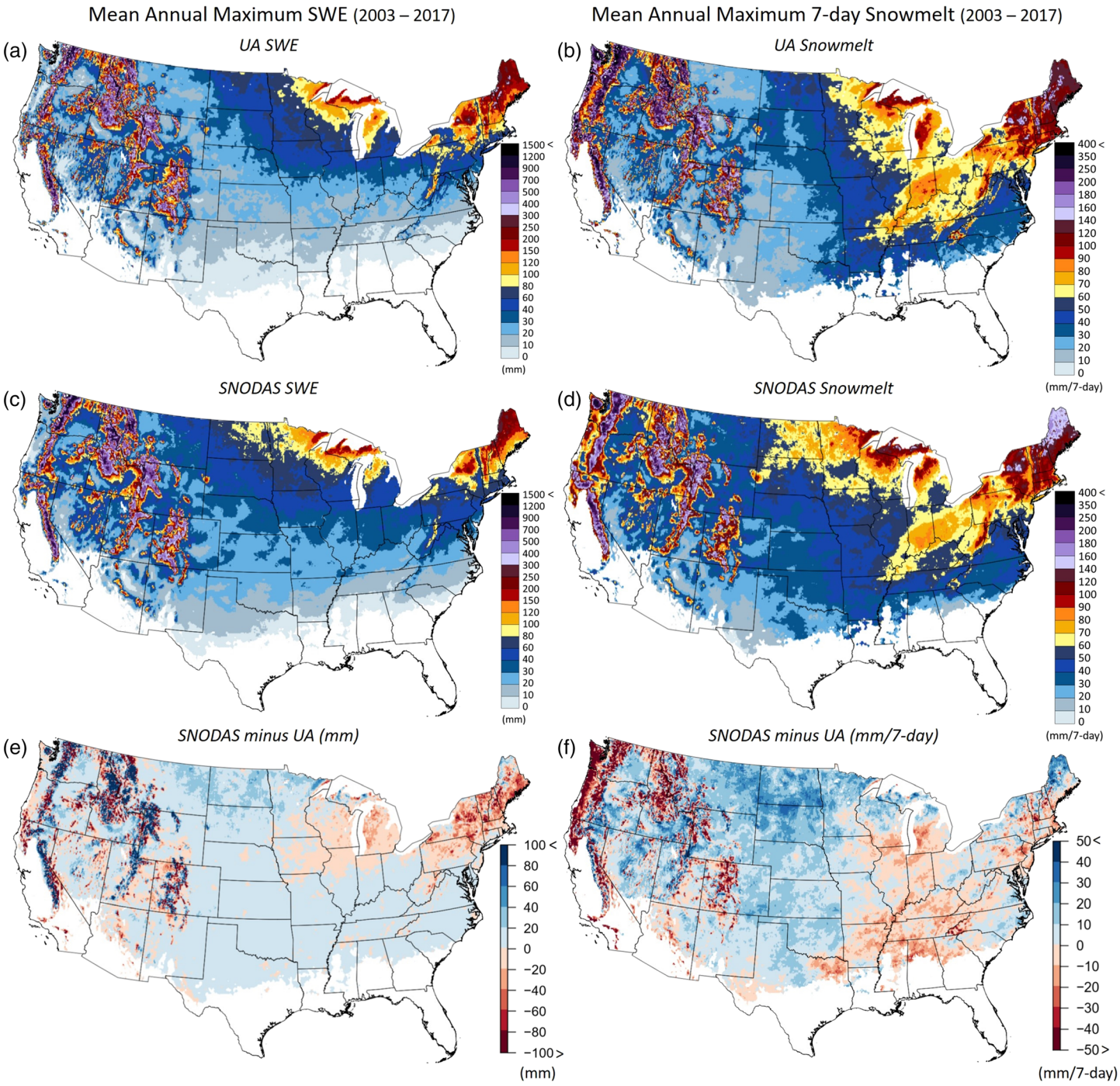

Figure 1. Mean annual maximum SWE and 7-day snowmelt maps from (a, b) UA and (c, d) SNODAS products, and (e, f) mean difference (SNODAS minus UA) maps in the SWE and 7-day snowmelt for the 14 years from October 2003 to May 2017.

average values by the state are similar but the extremes differ. While the state-mean values of UA snowmelt, 103, 118, and 57 mm, are slightly larger than SNODAS, 99, 100, and 58 mm, for Idaho, Washington, and Wyoming, the 99% quantile values are UA snowmelt values are consistently much larger than SNODAS values (UA: 274, 368, and 216 mm; SNODAS: 226, 279, and 168 mm, respectively). For readers who may be interested in additional maps, similar maps of the standard deviation and maximum values for the annual maximum SWE and the 7-day snowmelt are provided in the supporting information (Figures 2 and S1).

Table 1
Summary of the Mean Annual Maximum SWE and 7-Day Snowmelt From UA and SNODAS Products From 2003 to 2017 by U.S. States

	UA annual maximum SWE (mm)			SNODAS annual maximum SWE (mm)			UA annual maximum 7-day snowmelt (mm/7-day)			SNODAS annual maximum 7-day snowmelt (mm/7-day)		
State	Mean	Std	99%	Mean	Std	99%	Mean	Std	99%	Mean	Std	99%
Idaho	206	211	886	213	220	943	103	68	274	99	49	226
Maine	203	46	337	177	57	289	127	15	190	137	20	175
Washington	189	321	1,439	202	322	1,363	118	92	368	100	64	279
New Hampshire	167	61	345	132	49	268	120	26	200	114	20	169
Vermont	166	53	312	131	44	235	113	29	195	108	22	159
New York	115	53	280	93	39	216	95	24	168	97	23	162
Wyoming	111	176	797	121	179	753	57	52	216	58	37	168
Colorado	111	160	722	107	137	592	59	54	229	67	45	203
Montana	106	184	929	118	175	855	55	61	267	63	42	205
Oregon	99	175	918	93	141	722	82	17	125	83	23	142
Michigan	99	43	219	89	48	228	87	68	302	77	42	201
Massachusetts	97	31	178	78	23	153	105	14	146	97	14	126
Utah	83	111	532	89	119	559	53	44	203	56	39	181
Wisconsin	80	20	137	74	22	140	70	10	99	73	16	113
Minnesota	73	21	162	83	26	176	61	11	106	72	13	113
Connecticut	71	20	139	68	9	99	97	9	123	94	12	121
California	67	175	894	67	172	861	86	78	314	67	63	239
Rhode Island	64	13	84	61	10	75	99	9	115	88	8	100
Pennsylvania	63	21	114	55	13	88	75	13	110	74	13	110
North Dakota	52	12	74	70	12	94	44	9	59	64	8	81
New Jersey	47	17	96	43	13	69	77	14	110	66	11	95
Iowa	46	11	70	45	11	71	50	9	70	53	6	68
Nevada	43	55	277	43	52	250	35	26	142	40	22	121
West Virginia	41	27	142	40	18	99	69	15	123	69	15	117
South Dakota	37	12	71	49	14	84	36	7	61	54	9	81
Maryland	36	20	118	40	15	96	56	12	102	56	12	106
Ohio	34	11	75	38	7	68	68	7	86	70	6	84
Indiana	32	10	60	35	5	49	75	9	93	69	9	86
Illinois	31	13	61	32	6	51	59	9	83	55	6	70
Nebraska	26	5	39	33	5	44	47	2	50	55	1	57
Delaware	25	6	43	30	5	41	31	5	41	42	6	53
Virginia	24	9	57	29	8	48	53	4	62	51	3	57
New Mexico	22	4	34	28	3	34	48	11	79	48	8	72
Missouri	22	41	212	25	38	209	50	10	82	50	5	68
Kansas	20	3	28	28	3	34	21	19	111	25	15	93
Kentucky	20	4	30	26	4	34	27	6	41	37	5	51
Arizona	15	31	159	15	28	149	67	6	84	60	6	79
Tennessee	12	5	25	17	6	30	22	20	102	21	17	84
Arkansas	12	4	26	15	5	29	48	9	70	44	7	61
Oklahoma	11	4	21	21	5	29	56	10	86	49	8	68
North Carolina	11	7	42	16	7	33	40	15	100	40	8	65
Texas	4	3	13	8	5	19	26	6	44	35	5	47
South Carolina	4	4	17	7	7	25	28	9	51	27	8	43
Mississippi	3	2	12	5	3	11	19	9	45	19	9	36
Alabama	3	2	9	4	3	10	32	11	56	24	8	41
Georgia	2	3	13	4	5	21	36	8	55	32	8	58
Louisiana	1	1	4	3	2	7	22	11	62	20	10	55
Florida	—	—	—	—	—	—	—	—	—	—	—	—

Note. The states were arranged from the largest (top) to smallest (bottom) mean UA annual maximum SWE.

Figure 2's agreement statistics (R value) of annual maximum SWE and snowmelt between the two data products reflect the consistency between the products' low and high snow and snowmelt years from 2004 to 2017. For the annual maximum SWE, the spatial R value map typically shows strong agreement. In the north central and northeastern United States, the correlation is relatively high (>0.8) compared to the other regions. There is less agreement over parts of Montana, Wyoming, Nebraska, and Kansas, as well as the

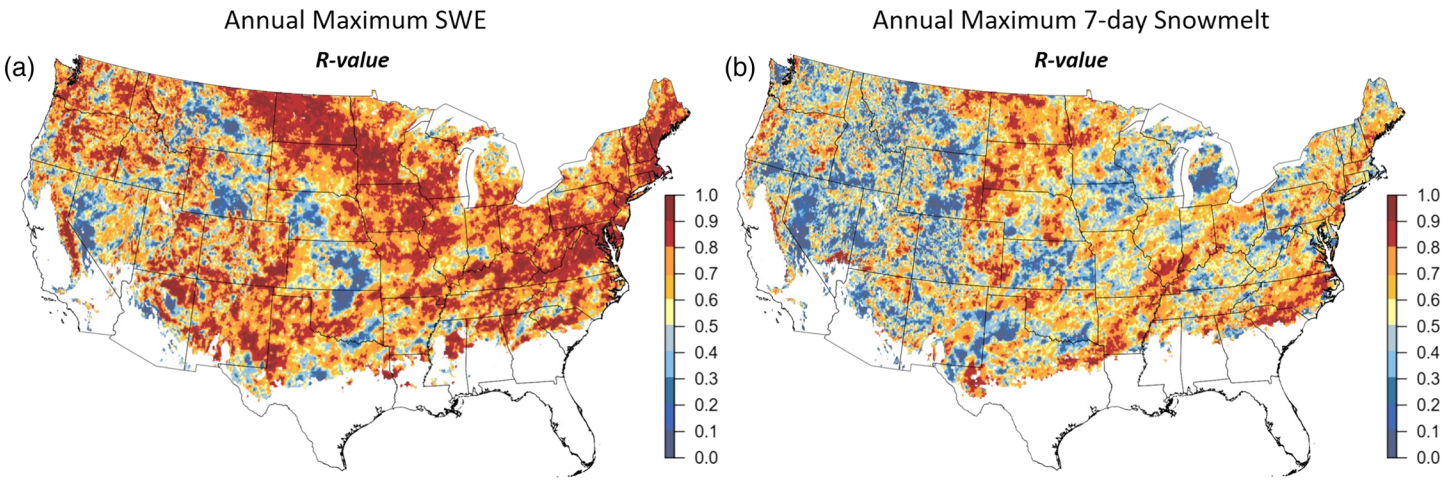

Figure 2. Pearson correlation (*R* value) maps of the (a) annual maximum SWE and (b) 7-day snowmelt between SNODAS and UA products for the 14 years from October 2003 to May 2017. Pixels with $N = 7$ or less available SWE or snowmelt were excluded.

western mountainous regions. The annual maximum snowmelt's agreement is not as strong as that for the annual maximum SWE comparison. The western and Midwest regions are notable for their poor agreement between annual maximum snowmelt values that were not evident in the annual maximum SWE agreement.

4.2. Extreme Design SWE and Snowmelt Maps Over the CONUS

After bias correcting and detrending the UA annual maximum SWE and snowmelt values, the extreme design SWE and 1- and 7-day snowmelt values are calculated (7-day extreme design snowmelt maps were focused here, and 1-day snowmelt maps were provided in the supporting information; Figure S3). The spatial patterns of the 25- and 100-year design SWE values are similar but differ in magnitude (Figure 3). The largest design SWE values, defined here as top 1% (99% quantile) values for each state, were found in western mountainous regions. For example, in Washington the top 1% 25- and 100-year return level SWE values are 2,713 and 3,542 mm, respectively. In the northeastern United States, the top 1% SWE values, 25-year values range from 443 to 639 mm, and, for 100-year value from 627 to 905 mm, are much lower than those in the mountainous western United States. However, the state-median values in the northeastern United States are higher than the western U.S. states. In the north central United States, the greatest design SWE values occur in the areas near Lake Michigan and the Red River of the North Basin along the Minnesota-North Dakota border. The top 1% values are 452 and 346 mm for the 25-year return level (654 and 512 mm for 100-year return level) in Michigan and Minnesota, respectively. For readers who may be interested in design maps using the original UA SWE without bias correction, the 25- and 100-year return level SWE maps are provided in the supporting information (Figures S4).

The 25- and 100-year snowmelt maps generally have similar spatial patterns to those of the annual maximum SWE maps (Figures 4a and 4b). Regions with high SWE are likely to also have large snowmelt events. The largest 7-day snowmelt values (top 1% for state) for 25- and 100-year return levels were also found in the western United States. The top 1% snowmelt values for 25-year return level range from 415 to 839 mm, and, from 615 to 1,547 mm for 100-year return level over the western mountainous regions including Washington, California, Idaho, and Oregon. In the northeastern United States, the magnitudes of the 25- and 100-year snowmelt are lower than that of the western United States. The northeastern's top 1% values for a 25-year range from 244 to 446 mm and, for 100-year, from 368 to 643 mm in Vermont, Maine, New Hampshire, and Massachusetts. The design snowmelt values in the north central United States are typically lower than that of the northeastern region. For 25- and 100-year, the top 1% snowmelt values are from 191 to 279 mm and from 330 to 447 mm, respectively, over the north central U.S. states including Michigan, Minnesota, South Dakota, and North Dakota.

To identify the effect of precipitation in estimating extreme snowmelt values, the 25- and 100-year 7-day snowmelt maps were compared to design values that do not include precipitation (Figures 4c and 4d).

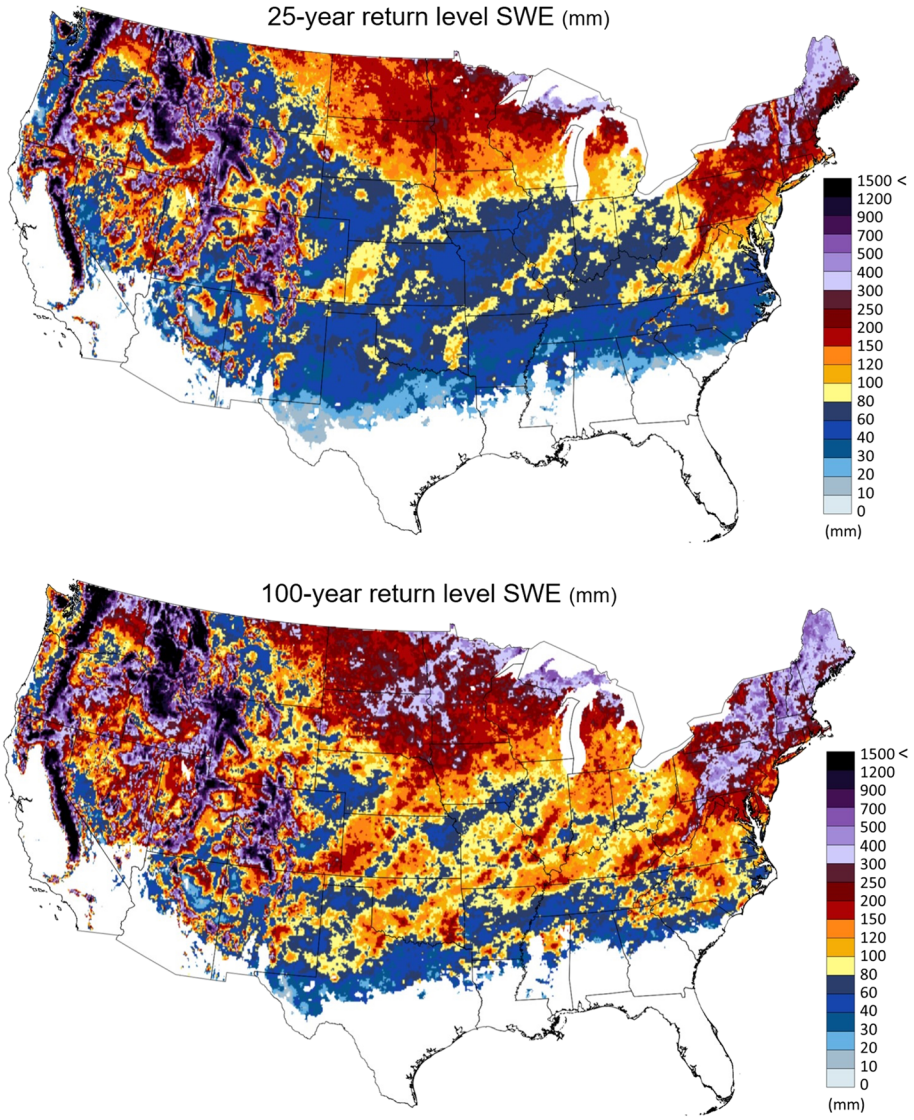

Figure 3. The (top) 25- and (bottom) 100-year return level design SWE maps using the detrended, ECDF-transformed annual maximum SWE.

Snowmelt without precipitation is calculated using a decrease in SWE only. The extreme snowmelt with precipitation is notably higher than the snowmelt without precipitation in the Pacific Northwest and California as well as the south central United States. For example, the highest 7-day, 100-year snowmelt values with precipitation are higher by 203, 206, and 260 mm for 25-year return level and, 362, 449, and 438 mm for 100-year return level, for Kansas, Oklahoma, and Tennessee respectively, as compared to the snowmelt values without precipitation (Figures 4e and 4f). In many snow-dominant regions including the western mountain, north-central, and northeastern regions, the extreme snowmelt with precipitation is also higher than the snowmelt without precipitation, indicating that precipitation during snowmelt is an important contributor to extreme snowmelt.

4.3. Design Snowmelt Versus NOAA Atlas 14 Precipitation

The design snowmelt maps were compared to the NOAA Atlas 14, 7-day duration precipitation maps for the 25- and 100-year return levels (Figure 5; the 1-day precipitation maps were compared to the corresponding design snowmelt maps in Figure S5). The design precipitation values are considerably larger than the design snowmelt values in the southern United States where there are few large snowmelt events. In the mountain

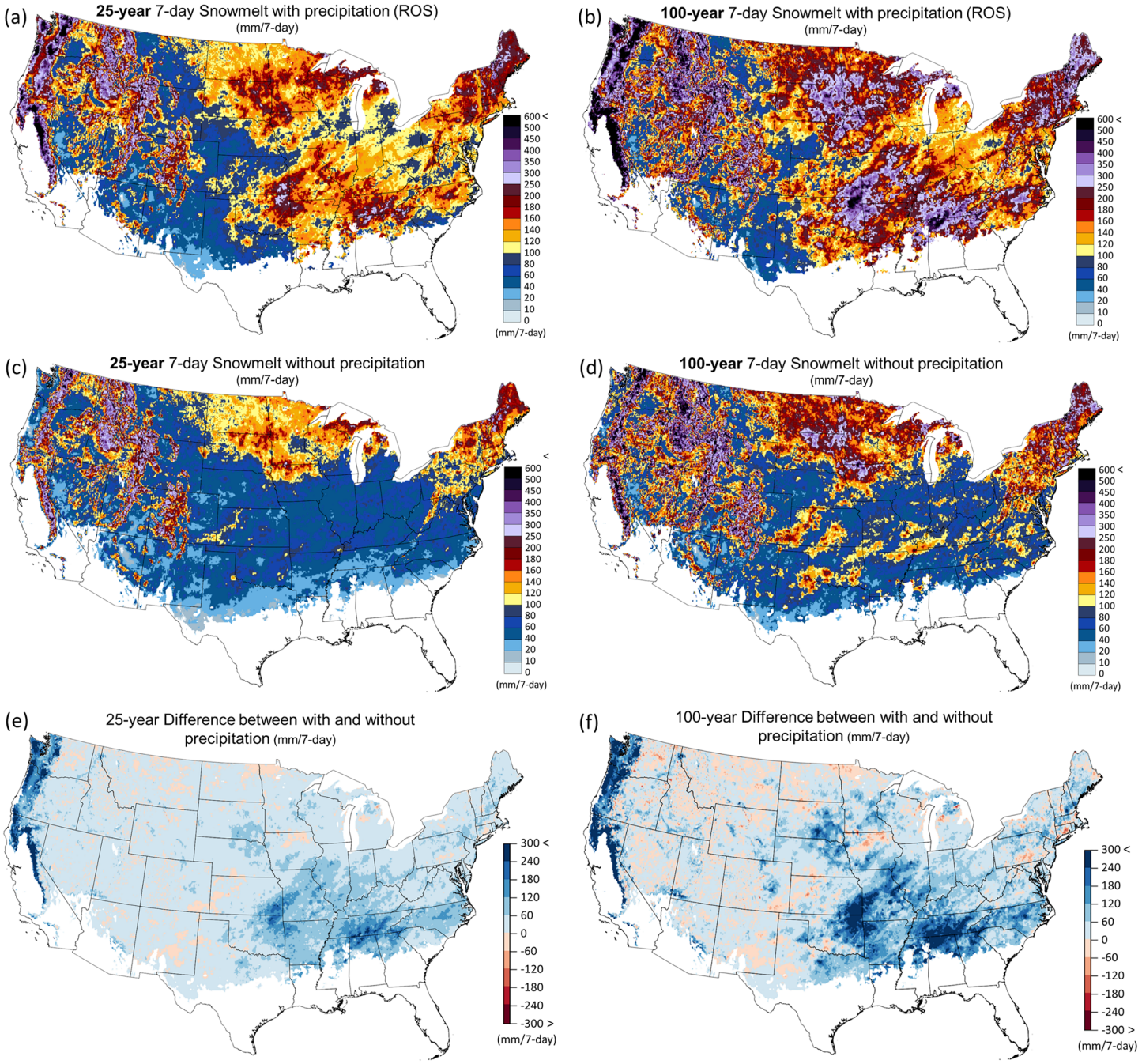

Figure 4. The (a, b) 25- and 100-year return level 7-day design snowmelt maps with precipitation and (c, d) without precipitation and (e, f) these differences (design 7-day snowmelt with precipitation minus without precipitation) over the CONUS.

western United States and the north-central United States, however, design snowmelt exceeded design precipitation. The 25- and 100-year difference maps consistently show that design snowmelt values are higher than Atlas 14 precipitation values over the mountain western United States. In the Northern Great Plains and upper Midwest, design snowmelt values are comparable to design precipitation values for the 25-year return period, but the 100-year snowmelt design values exceed the precipitation values in many parts of those regions. The inland portion of the northeastern states also has large regions where snowmelt values are modestly higher than precipitation values. There are several regions in the more southern regions including the Appalachian Mountain region where snowmelt exceeds the design rainfall despite the

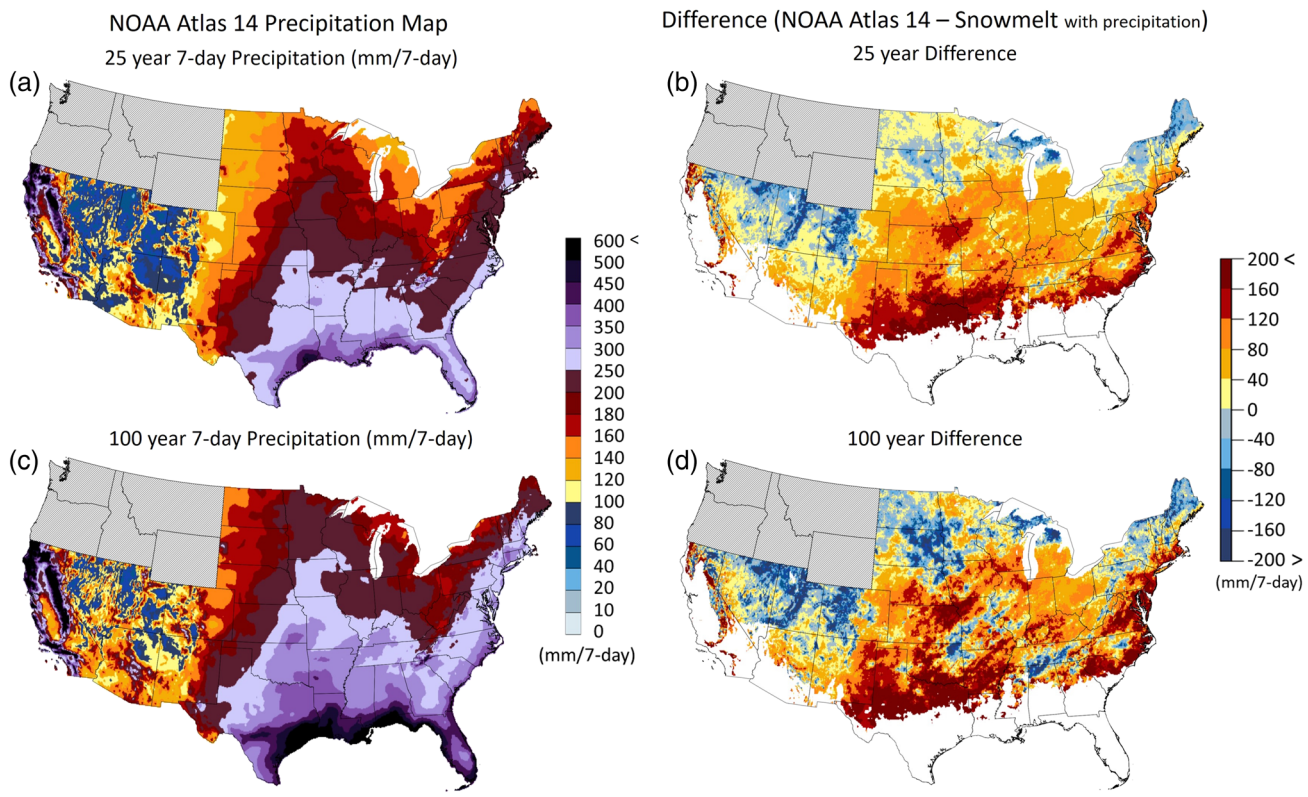

Figure 5. (a, c) The NOAA Atlas 14, 25- and 100-year 7-day precipitation maps, and (b, d) the difference maps (Atlas 14 minus corresponding snowmelt maps) over the CONUS. Cool colors indicate regions where the snowmelt values exceed the Atlas 14 precipitation values. The gray regions indicate U.S. states where annual maximum Atlas 14 data are not available. The white areas are out of range.

relatively low SWE values in those regions. This suggests that where the dominant source of meltwater during the ROS event is liquid precipitation, its amplification by the presence of a shallow snowpack may warrant consideration for design even in southern regions.

A more detailed comparison of design snowmelt from this study with the Atlas 14 standard precipitation was conducted for two regions that are historically vulnerable to snowmelt-driven floods (Berghuijs et al., 2016; Slater & Villarini, 2016; Stadnyk et al., 2016), the northeastern states (Atlas 14 Volume 10; Figure 6) and Midwest states (Atlas 14 Volume 8; Figure 7). In the northeastern United States, the Atlas 14 design precipitation values gradually decrease from the southeast to the northwest with the highest values in western Massachusetts and Connecticut as well as around Mount Washington in New Hampshire (Figures 6a and 6d). For the 25- and 100-year return periods, the precipitation depths in the southeastern areas range from about 134 (bottom 1%) to 277 mm (top 1%) and 160 to 357 mm, respectively, while in the northwestern areas precipitation values range from 109 to 280 mm and 124 to 495 mm for the 25- and the 100-year values, respectively. Although the snowmelt maps have larger spatial variability than the Atlas 14 precipitation maps (Figures 6b and 6e), design snowmelt values, as well as maximum SWE values, gradually increase from the southeast to the northwest. These design snowmelt gradients are inverse to the design precipitation gradients. The combination of higher SWE and more moderate design rainfall amplifies the importance of snowmelt-driven runoff in northern Vermont and Maine near the Canadian border, where design snowmelt can exceed design rainfall by up to 171 and 254 mm for the 25- and 100-year return periods, respectively.

In the Midwest United States, the NOAA Atlas 14 precipitation values are typically higher than the snowmelt values (Figure 7). In this region, the precipitation intensities decrease considerably to the northwest with ranges from 60 to 140 mm (25-year) and 80 to 230 mm (100-year). Western Colorado has the lowest design precipitation values. In locations with localized extremes at North and South Dakotas' eastern

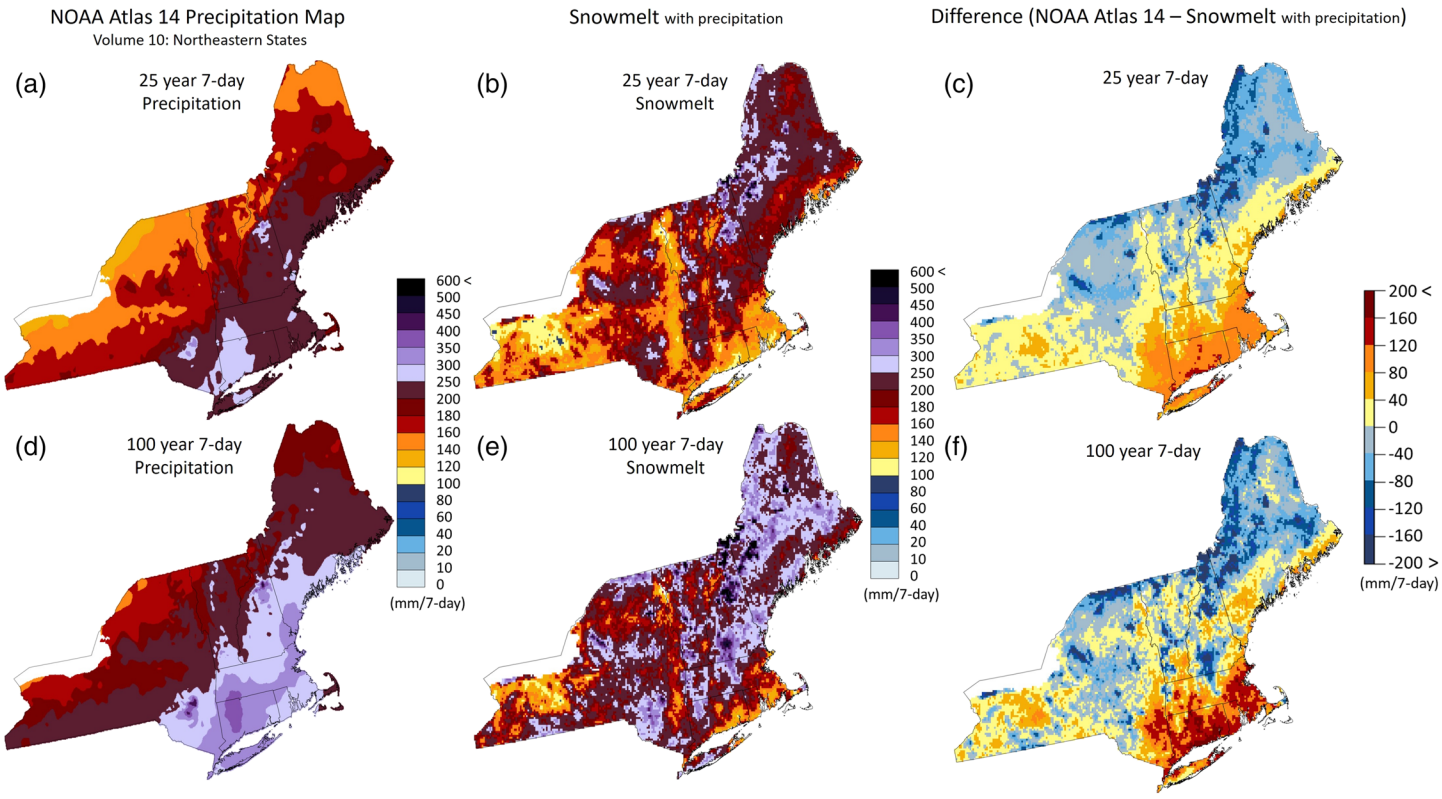

Figure 6. (a, d) The NOAA Atlas 14, 25- and 100-year 7-day precipitation maps, (b, e) the corresponding snowmelt maps, and (c, f) these differences (Atlas 14 minus snowmelt) over the northeastern U.S. including seven states (Massachusetts, New York, Vermont, New Hampshire, Maine, Rhode Island, and Connecticut).

borders, the border between Iowa and Minnesota, and Michigan's Upper Peninsula, the snowmelt magnitudes are higher than precipitation depth by up to 160 and 240 mm for the 25- and 100-year return periods, respectively (Figures 7c and 7f). In the Rocky Mountain region of western Colorado, the snowmelt magnitudes were markedly higher than the precipitation with difference up to 190 and 310 mm for the 25- and 100-year return periods, respectively. Interestingly, there are the localized extreme snowmelt values at Kansas and Oklahoma's eastern borders and southern Missouri. Although the 100-yr SWE values range from only 80 to 100 mm in the area, the design snowmelt values exceed 300 and 650 mm for 25- and 100- year return levels, respectively.

5. Discussion

5.1. Comparison Between UA and SNODAS Data

To date, no studies have directly compared the UA and SNODAS products over the CONUS, because the UA SWE data set was only recently publicly released (March 2019) via National Snow and Ice Data Center (Broxton et al., 2019). Broxton, Zeng, and Dawson (2016) showed that the reanalysis and GLDAS SWE products have considerably lower SWE than both UA and SNODAS SWE data. Their finding that SNODAS generally has higher SWE (and annual maximum SWE for 2008) than the UA product in Washington and Idaho as well as northern Great Plains, primarily for regions where the SWE is low, is consistent with our results. Dawson et al.'s (2017) study of snow density parameterization for developing the UA SWE product found that SNODAS snow densities have low biases compared to SNOTEL observations, particularly in ephemeral and maritime classes (11.1% and 16.2% of relative mean absolute error, respectively). They assert that these biases could be due to the assimilation of snow depth and SWE observations across different platforms and spatial scales (i.e., airborne gamma SWE, point-based snow depth and SWE observations, and satellite-based snow-covered area) without ingesting snow density observations.

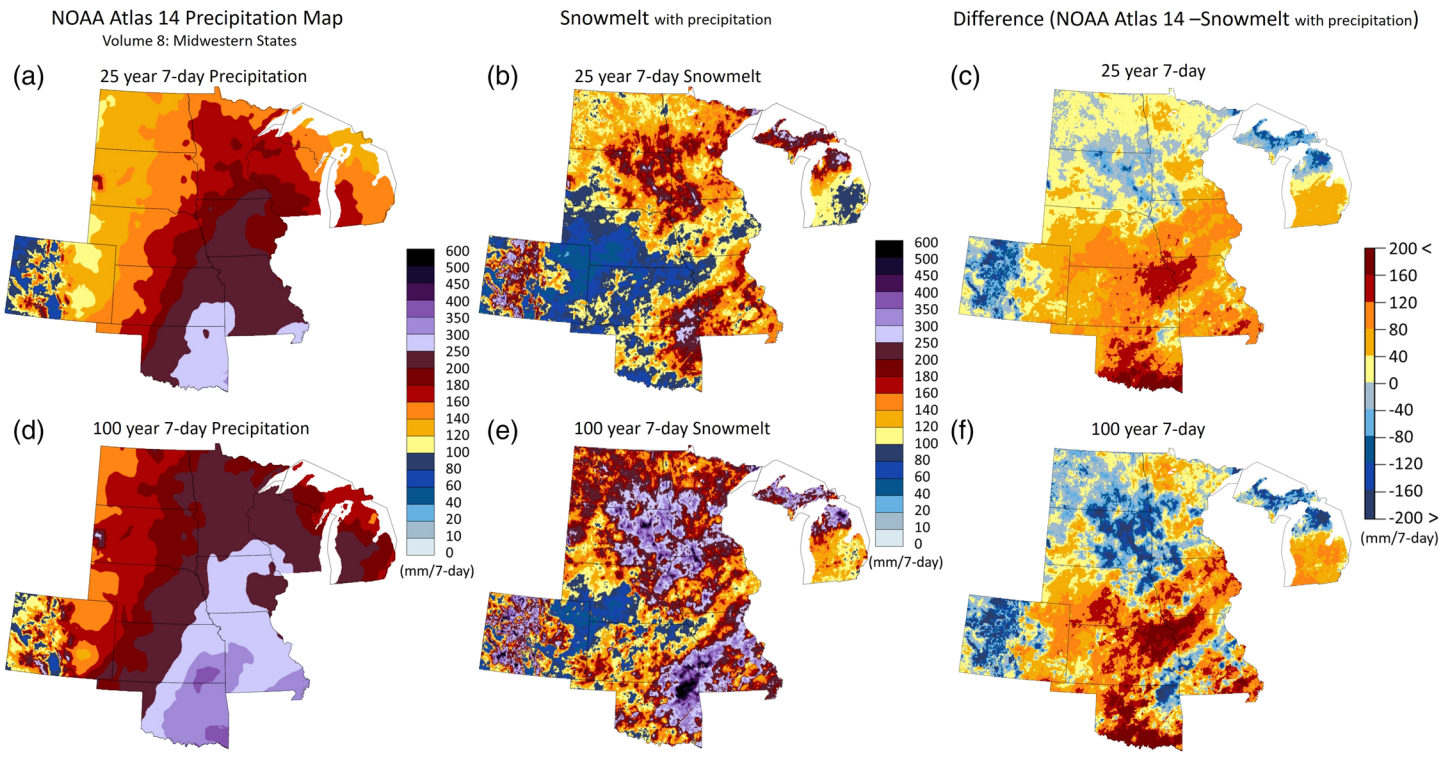

Figure 7. Same as Figure 6, but in the Midwest U.S. including 11 states (North Dakota, Minnesota, South Dakota, Nebraska, Colorado, Iowa, Missouri, Michigan, Kansas, Wisconsin, and Oklahoma).

Our findings that SNODAS snowmelt exceeded UA snowmelt over the north central and the western non-mountain United States may stem from the larger SNODAS annual maximum SWE compared to UA annual maximum SWE. The increased availability of SWE for melt may generate large snowmelt during the spring. However, in most western mountain regions, the UA annual maximum snowmelt exceeded the SNODAS despite the larger SNODAS SWE (Figure 8). Differences in the UA and SNODAS products' snow ablation procedures are likely responsible. The UA product calculates accumulated snow ablation using a simple cumulative degree day above 0°C method during the snow-covered period and generates SWE by subtracting accumulated snow ablation from accumulated snowfall (Broxton, Dawson, & Zeng, 2016). In contrast,

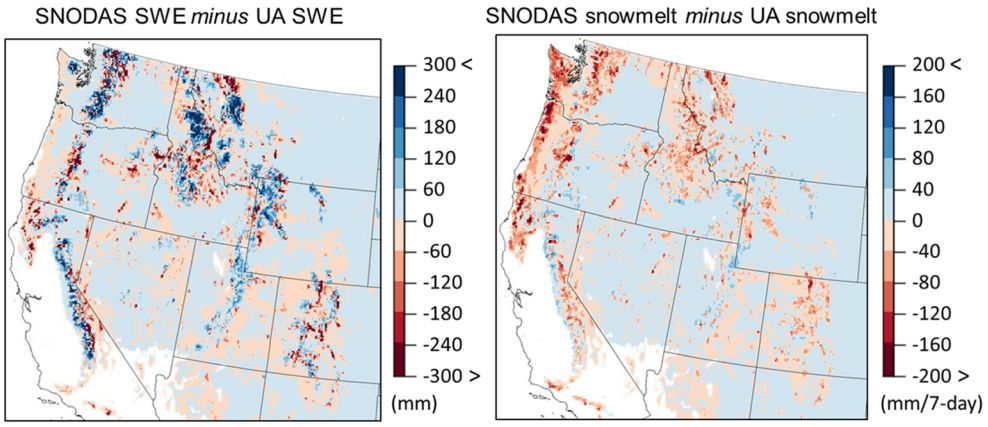

Figure 8. Same as Figures 1e and 1f (Mean difference maps of the annual maximum SWE and 7-day snowmelt) but changed the color bars ranging from −300 to 300 mm. Blue (red) color areas indicate that SNODAS is larger (smaller) than UA product.

SNODAS estimates snow ablation using the snow thermal model (SNTHERM.89) which tracks two variables, liquid water in the snowpack (state variable) and melt runoff rate at the base of the snowpack (diagnostic variable) (Barrett, 2003; Carroll, 2001). SNODAS considers both solid water and the liquid water in the snowpack as SWE. Thus, it is possible that the UA snowmelt may be overestimated, in part, due to the lack of liquid water storage in the snowpack.

5.2. Comparison to the NOAA Atlas 14 and the National Engineering Handbook

The current NOAA Atlas 14 volumes provides very limited guidance about snowmelt events (Perica et al., 2015, revised 2019). They focus on liquid precipitation (rainfall). Snowmelt events were not considered in the frequency estimates because this is a different runoff production mechanism. Unlike liquid precipitation, snowfall goes into storage (i.e., snowpack) and delays runoff until it melts. Our snowmelt estimates from this study complement the rainfall-based frequency estimates from the NOAA Atlas 14 series. From an engineering design perspective, the Atlas 14 design precipitation values are reasonable in regions where the Atlas 14 precipitation estimates equal or exceed our snowmelt estimates. However, in the areas where our snowmelt estimates are larger than the Atlas 14 precipitation values, infrastructure designed without consideration of snowmelt floods may underestimate design runoff and undersize structures. The maps presented in this study can provide guidance when developing flood defense structures in areas where major snowmelt floods have occurred over the past few decades (Changnon et al., 2001; Todhunter, 2001).

The National Engineering Handbook from United States Department of Agriculture Natural Resources Conservation Service (USDA NRCS) mapped snowmelt runoff volumes in the eastern Montana region (USDA-NRCS, 2004). Their 25-year, 7-day snowmelt runoff volumes ranged from 10 to 45 mm, which are much lower than the range of our snowmelt maps (40 to 140 mm) for the same region. The handbook also provided an example of a 25-year maximum 16–31 March SWE map in the north central United States, which was taken from a technical paper from U.S. Department of Commerce Weather Bureau (United States Department of Commerce, 1964). Their SWE values, ranging from 38 mm in the eastern Nebraska and South Dakota, to 305 mm near Lake Michigan, are somewhat lower than our SWE values for the same region (40–450 mm). The differences between these earlier maps are probably due, at least in part, to different time periods and data sets. Those maps used SWE or snow depth data obtained from several snow station networks with 15- to 55-year records (United States Department of Commerce, 1964) with a typical measurement period of 35 years from 1930 to 1964 as compared to UA's 1981 to 2017 record. There are differences not only in the SWE magnitude but also in the SWE spatial patterns. While the earlier maps showed that SWE gradually increased from southwestern (Nebraska and South Dakota) to northeastern parts of the region (e.g., Wisconsin and Michigan), our map shows very high SWE values in the headwaters of the Red River of the North Basin (near western Minnesota and southeastern North Dakota). This could be due to data limitations during the earlier time periods or to regional changes in snowfall under the changing climate (Byun et al., 2018; Hirsch & Ryberg, 2012). While there is little documentation about long-term SWE increases in that region, there is consensus that the Red River of the North Basin has experienced more frequent snowmelt flooding since the late 1990s (e.g., 1997, 2006, 2009, 2011, and 2019; Tuttle et al., 2017).

5.3. Limitations

Despite our efforts to combine the UA and SNODAS SWE products, regions where the annual maximum values from the two products have clear differences suggest inherent uncertainties. In this study, SNODAS SWE is assumed to be the most reliable data source over the CONUS based on previous studies (Broxton, Dawson, & Zeng, 2016; Broxton, Zeng, & Dawson, 2016; Vuyovich et al., 2014). Furthermore, the SNODAS data have been widely vetted by the NWS Regional River Forecast Centers for their use in operational flood forecasting (Barrett, 2003). However, recent studies have found that SNODAS SWE or snow depth has reduced performance in some regions as compared to independent data. Clow et al. (2012) showed that SNODAS SWE had a relatively poorer agreement ($R^2 = 0.30$) with in situ snow surveys in alpine areas, while SNODAS SWE performed well in forested areas ($R^2 = 0.77$) in Colorado Rocky Mountains. They indicated that wind redistribution of snow in alpine terrain may not be fully considered in a snow model in SNODAS, even though the SNODAS model is run with the surface zonal wind as a driving variable (Barrett, 2003). While not yet studied, because the interpolation and assimilation processes for UA

SWE do not account for wind effects, it is reasonable that wind redistribution would also impact the UA SWE estimates. Anderson (2011) also found that SNODAS underestimated snow depths in forested alpine terrain. Hedrick et al.'s (2015) evaluation of SNODAS snow depth using lidar-based snow depth measurements during the 2007 Colorado Cold Lands Processes Experiment (CLPX-2) also found regional differences between the two snow depth products, especially in the areas with dense low sagebrush where high winds scour the snow throughout the winter. Boniface et al. (2015), conducting a comparison study of SNODAS snow depth with the Global Positioning System Interferometric Reflectometry (GPS-IR)-based snow depth observations over the western United States, found that there were clear differences between the two snow depth products in areas with complex terrain or strong vegetation heterogeneities.

In the upper Tuolumne River Basin in California's Sierra Nevada, comparison results of the ASO SWE with SNODAS SWE showed that SNODAS overestimated SWE during the melt phase (Bair et al., 2016). However, they could not determine the mechanism that caused the errors because few publications address the details of the snow model structure and assimilation scheme in SNODAS. Dozier et al. (2016) suggested a potential cause for the overestimates is that the snow pillows, whose measurements are assimilated in SNODAS, could hold more SWE than the average of the surrounding terrain because they hinder drainage of melted water to the underlying soil. Given that UA SWE mainly ingests snow pillow measurements from the SNOTEL network over the western United States (Zeng et al., 2018), snow pillows may also be a source of uncertainties in UA SWE product.

Lastly, there are inevitable limitations related to the available data length issue for bias correction (14-year overlap period) and frequency analysis (36-year period). If longer periods were available for the UA and SNODAS SWE products, then the frequency distribution would be more precisely determined, and the design values may be statistically more robust than the current values (Stedinger et al., 1993).

6. Conclusion

The current engineering practice (e.g., NOAA Atlas 14) provides limited guidance on designing infrastructure to accommodate snowmelt-driven floods in the CONUS. In this study, we leverage two vetted, long-term CONUS SWE products from the UA and SNODAS to develop 25- and 100-year return level design SWE and snowmelt maps. Extreme value statistical methods are used to fit the GEV distribution to detrended, bias-corrected annual maximum SWE and snowmelt values from a 36-year record (water years 1982 to 2017).

Despite their use of different methods to estimate SWE, the UA and SNODAS annual maximum SWE products are strongly correlated indicating that year-to-year variations in annual maximum SWE values are readily distinguished. There is notably less agreement between the two products' year-to-year snowmelt patterns. This suggests a need for additional study regarding more reliable approaches for estimating snowmelt at time and space scales that are appropriate for design. Much of the study region had a reasonable agreement for the magnitude of the annual maximums. The SWE and 7-day snowmelt design maps show similar patterns and, as anticipated, regions having larger annual maximum SWE values typically also have greater snowmelt. The 7-day design snowmelt values exceed the NOAA Atlas 14 standard design values in 23% of the total extent. Especially in the northeastern United States near the Canadian border, the north central United States where just 10 cm of SWE can cause spring flooding, and the western mountainous United States, design snowmelt substantially exceeds the Atlas 14 design precipitation values.

Additionally, a comparison of design snowmelt values with and without precipitation shows that the extreme snowmelt with precipitation is notably higher than the snowmelt without precipitation in the Pacific Northwest, California, and the south-central United States. In most snow-dominant regions, the extreme snowmelt with precipitation is generally higher than the snowmelt without precipitation, indicating that precipitation events during snowmelt (e.g., ROS) are an important contributor to extreme snowmelt. The extreme snowmelt CONUS maps from this study complement the NOAA Atlas 14 design precipitation and may provide additional guidance on infrastructure design for compound flood events over snow-dominant regions in the CONUS.

Data Availability Statement

The daily UA SWE data are freely available from the National Snow and Ice Data Center (NSIDC) website (https://nsidc.org/data/nsidc-0719). The daily SNODAS SWE and solid and liquid precipitation data are also available from the NSIDC website (https://nsidc.org/data/G02158). The daily PRISM precipitation data can be obtained using the "get_prism_dailys" function in the "prism" R package (https://github.com/ropensci/prism) or the PRISM Climate Group website (http://prism.oregonstate.edu/recent/). The standard NOAA Atlas 14 precipitation maps are available from the Hydrometeorological Design Studies Center (HDSC) within the Office of Water Prediction (OWP) of the NOAA's National Weather Service (NWS) (https://hdsc.nws.noaa.gov/hdsc/pfds/pfds_gis.html). The design SWE and snowmelt maps from this study are available on Hydroshare at this website (http://www.hydroshare.org/resource/c50069a2e1fa43418d1ee75c0e92313e).

Acknowledgments

We would like to thank the WRR editorial team including Martyn Clark (Editor-in-Chief), Erkan Istanbulluoglu (Associate Editor), and three anonymous reviewers for taking their time to provide constructive comments that greatly improved this paper. We are grateful to Eunsang Cho's Ph.D. committee members, Ernst Linder, Carrie Vuyovich, Anne Lightbody, and Jo Sias, who gave insightful comments on an earlier version of the paper that have resulted in significant improvements. The authors gratefully acknowledge support from NASA Water Resources Applied Sciences Program (NNX15AC47G). Eunsang Cho was also supported by 2019–2020 Dissertation Year Fellowship (DYF) from University of New Hampshire.

References

American National Standards Institute (1972). Building code requirements for minimum design loads in buildings and other structures. ANSI A58.1–1972, New York.

American Society of Civil Engineers (2017). Minimum design loads and associated criteria for buildings and other structures. ASCE/SEI 7–16, Reston, VA.

Anderson, B. T. (2011). Spatial distribution and evolution of a seasonal snowpack in complex terrain: An evaluation of the SNODAS modeling product, *Masters thesis, Boise State University*, Boise, Idaho, USA.

Bair, E. H., Rittger, K., Davis, R. E., Painter, T. H., & Dozier, J. (2016). Validating reconstruction of snow water equivalent in California's Sierra Nevada using measurements from the NASA Airborne Snow Observatory. *Water Resources Research*, *52*, 8437–8460. https://doi.org/10.1002/2016WR018704

Barrett, A. P. (2003). *National operational hydrologic remote sensing center snow data assimilation system (SNODAS) products at NSIDC* (p. 19). Boulder, CO: National Snow and Ice Data Center, Cooperative Institute for Research in Environmental Sciences.

Bean, B., Maguire, M., & Sun, Y. (2019). Comparing design ground snow load prediction in Utah and Idaho. *Journal of Cold Regions Engineering*, *33*, 04019010. https://doi.org/10.1061/(ASCE)CR.1943-5495.0000190

Berghuijs, W. R., Woods, R. A., Hutton, C. J., & Sivapalan, M. (2016). Dominant flood generating mechanisms across the United States. *Geophysical Research Letters*, *43*, 4382–4390. https://doi.org/10.1002/2016GL068070

Boniface, K., Braun, J. J., McCreight, J. L., & Nievinski, F. G. (2015). Comparison of snow data assimilation system with GPS reflectometry snow depth in the western United States. *Hydrological Processes*, *29*(10), 2425–2437. https://doi.org/10.1002/hyp.10346

Bonnin, G. M., Martin, D., Lin, B., Parzybok, T., Yekta, M., & Riley, D. (2006). NOAA Atlas 14 volume 2 version 3, Precipitation-Frequency Atlas of the United States, Ohio River basin and surrounding States. NOAA, National Weather Service, Silver Spring, MD.

Broxton, P., Dawson, N., & Zeng, X. (2016). Linking snowfall and snow accumulation to generate spatial maps of SWE and snow depth. *Earth and Space Science*, *3*, 246–256. https://doi.org/10.1002/2016EA000174

Broxton, P., Zeng, X., & Dawson, N. (2016). Why do global reanalyses and land data assimilation products underestimate snow water equivalent? *Journal of Hydrometeorology*, *17*(11), 2743–2761. https://doi.org/10.1175/JHM-D-16-0056.1

Broxton, P., Zeng, X., & Dawson, N. (2019). Daily 4 km gridded SWE and snow depth from assimilated in-situ and modeled data over the conterminous US, version 1. Boulder, Colorado USA. NASA National Snow and Ice Data Center Distributed Active Archive Center. https://doi.org/10.5067/0GGPB220EX6A. [accessed on 1 May, 2019].

Byun, K., Chiu, C.-M., & Hamlet, A. F. (2018). Effects of 21st century climate change on seasonal flow regimes and hydrologic extremes over the Midwest and Great Lakes region of the US. *Science of The Total Environment*, *650*(Pt 1), 1261–1277. https://doi.org/10.1016/j.scitotenv.2018.09.063

Carroll, T., Cline, D., Olheiser, C., Rost, A., Nilsson, A., Fall, G., et al. (2006). NOAA's national snow analyses, Proc. Western Snow Conference, Las Cruces, NM, vol. 74. [Available at www.westernsnowconference.org/sites/westernsnowconference.org/PDFs/2006Carroll.pdf.]

Carroll, T. R. (2001). Airborne gamma radiation snow survey program: A user's guide, version 5.0. National Operational Hydrologic Remote Sensing Center (NOHRSC), Chanhassen, 14.

Changnon, S. A., Kunkel, K. E., & Andsager, K. (2001). Causes for record high flood losses in the central United States. *Water International*, *26*(2), 223–230. https://doi.org/10.1080/02508060108686908

Cheng, L., & AghaKouchak, A. (2014). Nonstationary precipitation intensity-duration-frequency curves for infrastructure design in a changing climate. *Scientific Reports*, *4*, 7093. https://doi.org/10.1038/srep07093

Cho, E., Jacobs, J. M., & Vuyovich, C. (2019). The value of long-term (40 years) airborne gamma radiation SWE record for evaluating three observation-based gridded SWE datasets by seasonal snow and land cover classifications. *Water Resources Research*, *56*, e2019WR025813. https://doi.org/10.1029/2019WR025813

Chowdhury, J. U., Stedinger, J. R., & Lu, L.-H. (1991). Goodness-of-fit tests for regional generalized extreme value flood distributions. *Water Resources Research*, *27*(7), 1765–1776. https://doi.org/10.1029/91WR00077

Clow, D. W., Nanus, L., Verdin, K. L., & Schmidt, J. (2012). Evaluation of SNODAS snow depth and snow water equivalent estimates for the Colorado Rocky Mountains, USA. *Hydrological Processes*, *26*(17), 2583–2591. https://doi.org/10.1002/hyp.9385

Daly, C., Halbleib, M., Smith, J. I., Gibson, W. P., Doggett, M. K., Taylor, G. H., et al. (2008). Physiographically sensitive mapping of climatological temperature and precipitation across the conterminous United States. *International Journal of Climatology*, *28*(15), 2031–2064. https://doi.org/10.1002/joc.1688

Davenport, F. V., Herrera-Estrada, J. E., Burke, M., & Diffenbaugh, N. S. (2020). Flood size increases nonlinearly across the Western United States in response to lower snow-precipitation ratios. *Water Resources Research*, *56*, e2019WR025571. https://doi.org/10.1029/2019WR025571

Dawson, N., Broxton, P., & Zeng, X. (2017). A new snow density parameterization for land data assimilation. *Journal of Hydrometeorology*, *18*(1), 197–207. https://doi.org/10.1175/JHM-D-16-0166.1

Dawson, N., Broxton, P., & Zeng, X. (2018). Evaluation of remotely-sensed snow water equivalent and snow cover extent over the contiguous United States. *Journal of Hydrometeorology*, *19*(11), 1777–1791. https://doi.org/10.1175/JHM-D-18-0007.1

Dozier, J., Bair, E. H., & Davis, R. E. (2016). Estimating the spatial distribution of snow water equivalent in the world's mountains. *WIREs Water*, *3*(3), 461–474. https://doi.org/10.1002/wat2.1140

Fassnacht, S. R., & Records, R. M. (2015). Large snowmelt versus rainfall events in the mountains. *Journal of Geophysical Research: Atmospheres*, *120*, 2375–2381. https://doi.org/10.1002/2014JD022753

Federal Emergency Management Agency (2012). Summary of existing guidelines for hydrologic safety of dams. https://www.fema.gov/media-library-data/20130726-1849-25045-9688/04_hydrosafetydam_ch_9_11.pdf

Filliben, J. J. (1975). The probability plot correlation coefficient test for normailty. *Technometrics*, *17*(1), 111–117. https://doi.org/10.1080/00401706.1975.10489279

Geis, J., Strobel, K., & Liel, A. (2012). Snow-induced building failures. *Journal of Performance of Constructed Facilities*, *26*(4), 377–388. https://doi.org/10.1061/(ASCE)CF.1943-5509.0000222

Harpold, A. A., & Kohler, M. (2017). Potential for changing extreme snowmelt and rainfall events in the mountains of the western United States. *Journal of Geophysical Research: Atmospheres*, *122*, 13–219. https://doi.org/10.1002/2017JD027704

Hedrick, A., Marshall, H. P., Winstral, A., Elder, K., Yueh, S., & Cline, D. (2015). Independent evaluation of the SNODAS snow depth product using regional-scale lidar-derived measurements. *The Cryosphere*, *9*(1), 13–23. https://doi.org/10.5194/tc-9-13-2015

Henn, B., Musselman, K. N., Lestak, L., Ralph, F. M., & Molotch, N. P. (2020). Extreme runoff generation from atmospheric river driven snowmelt during the 2017 Oroville Dam spillways incident. *Geophysical Research Letters*, *47*, e2020GL088189. https://doi.org/10.1029/2020GL088189

Hirsch, R. M., & Ryberg, K. R. (2012). Has the magnitude of floods across the USA changed with global CO_2 levels. *Hydrological Sciences Journal*, *57*(1), 1–9. https://doi.org/10.1080/02626667.2011.621895

Hosking, J. R. M. (1990). L-moments: Analysis and estimation of distributions using linear combinations of order statistics. *Journal of the Royal Statistical Society: Series B: Methodological*, *52*(1), 105–124.

Hosking, J. R. M., Wallis, J. R., & Wood, E. F. (1985). Estimation of the generalized extreme-value distribution by the method of probability-weighted moments. *Technometrics*, *27*(3), 251–261. https://doi.org/10.1080/00401706.1985.10488049

Ivancic, T. J., & Shaw, S. B. (2015). Examining why trends in very heavy precipitation should not be mistaken for trends in very high river discharge. *Climatic Change*, *133*, 681–693. https://doi.org/10.1007/s10584-015-1476-1

Kendall, M. G. (1938). A new measure of rank correlation. *Biometrika*, *30*(1/2), 81–93. https://doi.org/10.2307/2332226

Khaliq, M. N., Ouarda, T. B. M. J., Ondo, J. C., Gachon, P., & Bobée, B. (2006). Frequency analysis of a sequence of dependent and/or nonstationary hydro-meteorological observations: A review. *Journal of Hydrology*, *329*(3–4), 534–552. https://doi.org/10.1016/j.jhydrol.2006.03.004

Li, D., Lettenmaier, D. P., Margulis, S. A., & Andreadis, K. (2019). The role of rain-on-snow in flooding over the conterminous United States. *Water Resources Research*, *55*, 8492–8513. https://doi.org/10.1029/2019WR024950

Looney, S. W., & Gulledge, T. R. Jr. (1985). Use of the correlation coefficient with normal probability plots. *The American Statistician*, *39*(1), 75–79.

Mann, H. B. (1945). Nonparametric tests against trend. *Econometrica: Journal of the Econometric Society*, *13*(3), 245–259. https://doi.org/10.2307/1907187

McGinnis, S., Nychka, D., & Mearns, L. O. (2015). A new distribution mapping technique for climate model bias correction. In *Machine learning and data mining approaches to climate science* (pp. 91–99). Cham: Springer. https://doi.org/10.1007/978-3-319-17220-0_9

Musselman, K. N., Clark, M. P., Liu, C., Ikeda, K., & Rasmussen, R. (2017). Slower snowmelt in a warmer world. *Nature Climate Change*, *7*(3), 214–219. https://doi.org/10.1038/nclimate3225

Musselman, K. N., Lehner, F., Ikeda, K., Clark, M. P., Prein, A. F., Liu, C., et al. (2018). Projected increases and shifts in rain-on-snow flood risk over western North America. *Nature Climate Change*, *8*(9), 808–812. https://doi.org/10.1038/s41558-018-0236-4

Perica, S., Martin, D., Pavlovic, S., Roy, I., St. Laurent, M., Trypaluk, C., et al. (2013). NOAA Atlas 14 volume 8 version 2, Precipitation-Frequency Atlas of the United States, Midwestern States. NOAA, National Weather Service, Silver Spring, MD.

Perica, S., Pavlovic, S., St Laurent, M., Trypaluk, C., Unruh, D., Martin, D., Wilhite, O. (2015, revised 2019). NOAA Atlas 14 volume 10 version 3, Precipitation-Frequency Atlas of the United States, Northeastern States. NOAA, National Weather Service, Silver Spring, MD.

Sack, R. L. (2015). Ground snow loads for the Western United States: State of the art. *Journal of Structural Engineering*, *142*, 04015082. https://doi.org/10.1061/(ASCE)ST.1943-541X.0001343

Schroeder, R., Jacobs, J. M., Cho, E., Olheiser, C. M., DeWeese, M. M., Connelly, B. A., et al. (2019). Comparison of satellite passive microwave with modeled snow water equivalent estimates in the Red River of the North Basin. *IEEE Journal of Selected Topics in Applied Earth Observations and Remote Sensing*, *12*(9), 3233–3246. https://doi.org/10.1109/JSTARS.2019.2926058

Sen, P. K. (1968). Robustness of some nonparametric procedures in linear models. *The Annals of Mathematical Statistics*, *39*(6), 1913–1922. https://doi.org/10.1214/aoms/1177698021

Serreze, M. C., Clark, M. P., Armstrong, R. L., McGinnis, D. A., & Pulwarty, R. S. (1999). Characteristics of the western United States snowpack from Snowpack Telemetry (SNOTEL) data. *Water Resources Research*, *35*(7), 2145–2160. https://doi.org/10.1029/1999WR900090

Slater, L. J., & Villarini, G. (2016). Recent trends in U.S. flood risk. *Geophysical Research Letters*, *43*, 12,428–12,436. https://doi.org/10.1002/2016GL071199

Stadnyk, T., Dow, K., Wazney, L., & Blais, E.-L. (2016). The 2011 flood event in the Red River basin: causes, assessment and damages. *Canadian Water Resources Journal*, *41*(1–2), 56–64. https://doi.org/10.1080/07011784.2015.1009949

Stedinger, J. R., Vogel, R. M., & Foufoula-Georgiou, E. (1993). Chapter 18 Frequency Analysis of Extreme Events. In D. R. Maidment (Ed.), *Handbook of Hydrology* (pp. 1–66). New York: DR McGraw-Hill. https://sites.tufts.edu/richardvogel/files/2019/04/frequencyAnalysis.pdf

Takala, M., Luojus, K., Pulliainen, J., Derksen, C., Lemmetyinen, J., Kärnä, J. P., et al. (2011). Estimating northern hemisphere snow water equivalent for climate research through assimilation of space-borne radiometer data and ground-based measurements. *Remote Sensing of Environment*, *115*(12), 3517–3529. https://doi.org/10.1016/j.rse.2011.08.014

Todhunter, P. E. (2001). A hydroclimatological analysis of the Red River of the North snowmelt flood catastrophe of 1997. *JAWRA Journal of the American Water Resources Association*, *37*(5), 1263–1278. https://doi.org/10.1111/j.1752-1688.2001.tb03637.x

Tuttle, S. E., Cho, E., Restrepo, P. J., Jia, X., Vuyovich, C. M., Cosh, M. H., & Jacobs, J. M. (2017). Remote sensing of drivers of spring snowmelt flooding in the North Central U.S. In V. Lakshmi (Ed.), *Remote sensing of hydrological extremes*, *Springer Remote Sensing/Photogrammetry* (pp. 21–45). Cham: Springer. https://doi.org/10.1007/978-3-319-43744-6_2

United States Department of Commerce (1964). Frequency of maximum water equivalent of March snow cover in North Central United States. Weather Bureau, Technical Paper, No. 50, Washington, DC. https://www.nws.noaa.gov/oh/hdsc/Technical_papers/TP50.pdf

USDA-NRCS (2004). Chapter 11 Snowmelt. Part 630 Hydrology National Engineering Handbook (pp. 1–21). Washington DC, USA: USDA Natural Resources Conservation Service. https://directives.sc.egov.usda.gov/OpenNonWebContent.aspx?content=17753.wba

Villarini, G. (2016). On the seasonality of flooding across the continental United States. *Advances in Water Resources*, *87*, 80–91. https://doi.org/10.1016/j.advwatres.2015.11.009

Vogel, R. M., & Fennessey, N. M. (1993). L moment diagrams should replace product moment diagrams. *Water Resources Research*, *29*(6), 1745–1752. https://doi.org/10.1029/93WR00341

Vuyovich, C. M., Jacobs, J. M., & Daly, S. F. (2014). Comparison of passive microwave and modeled estimates of total watershed SWE in the continental United States. *Water Resources Research*, *50*, 9088–9102. https://doi.org/10.1002/2013WR014734

Wazney, L., & Clark, S. P. (2015). The 2009 flood event in the Red River Basin: Causes, assessment and damages. *Canadian Water Resources Journal*, *41*(1–2), 56–64. https://doi.org/10.1080/07011784.2015.1009949

Yan, H., Sun, N., Wigmosta, M., Leung, L. R., Hou, Z., Coleman, A., & Skaggs, R. (2019). Evaluating next-generation intensity-duration-frequency curves for design flood estimates in the snow-dominated western United States. *Hydrological Processes*, *34*(5), 1255–1268. https://doi.org/10.1002/hyp.13673

Yan, H., Sun, N., Wigmosta, M., & Skaggs, R. (2019). Next-generation intensity-duration-frequency curves to reduce errors in peak flood design. *ASCE Journal of Hydrologic Engineering*, *24*, 04019020. https://doi.org/10.1061/(ASCE)HE.1943-5584.0001799

Yan, H., Sun, N., Wigmosta, M., Skaggs, R., Hou, Z., & Leung, R. (2018). Next-generation intensity-duration-frequency curves for hydrologic design in snow-dominated environments. *Water Resources Research*, *54*, 1093–1108. https://doi.org/10.1002/2017WR021290

Zeng, X., Broxton, P., & Dawson, N. (2018). Snowpack change from 1982 to 2016 over conterminous United States. *Geophysical Research Letters*, *45*, 12,940–12,947. https://doi.org/10.1029/2018GL079621